Research Square

Preprints are preliminary reports that have not undergone peer review.
They should not be considered conclusive, used to inform clinical practice,
or referenced by the media as validated information.

A case study: Study on the fracture evolution of overlying strata and the law of surface subsidence caused by coal resource mining

Su shijie
Taiyuan University of Technology
Wang kai
tywk2008@163.com

Taiyuan University of Technology
Li wenbo
Taiyuan University of Technology
Ding guoli
Zhongtian Hechuang Energy Co., Ltd
Qiu pengqi
Taiyuan University of Technology
Zhang xiaoqiang
Taiyuan University of Technology
Han gang
China Coal Energy Research Institute Co., Ltd. Xian
Jiang yulong
Taiyuan University of Technology

Article

Keywords: coal resources, large mined-out area, microseism, overburden strata, ground surface subsidence, secondary activation

Posted Date: November 10th, 2026

DOI: https://doi.org/10.21203/rs.3.rs-11369575/v1

License: This work is licensed under a Creative Commons Attribution 4.0 International License.
Read Full License

Additional Declarations: No competing interests reported.

Title: A case study: Study on the fracture evolution of overlying strata and the law of surface subsidence caused by coal resource mining

Su shijie[12], Wang kai[1*], Li wenbo[1], Ding guoli[3], Qiu pengqi[1],Zhang xiaoqiang[1], Han gang[4], Jiang yulong[1]

1 School of Mining Engineering, Taiyuan University of Technology, Taiyuan 030024,China

2 China Coal Energy Company Limited., Beijing 100120,China

3 Zhongtian Hechuang Energy Co., Ltd, Ordos, Inner Mongolia 017317,China

4 China Coal Energy Research Institute Co., Ltd. Xian, 710000,China

Corresponding author: Wang kai , e-mail: tywk2008@163.com

Research funding: No, this research did not receive funding.

Abstract : The continuous goaf area formed by coal resource mining is too large, which makes the roof movement characteristics of goaf become extremely complex. Based on the engineering background of 3104,3106 and 3107 working faces in Menkeqing Coal Mine, this paper studies the roof activity and surface subsidence of large goaf. In this study, microseismic monitoring, 3DEC numerical simulation and field measurement methods were used to analyze the overburden movement and surface subsidence of large goaf. The results show that with the advance of mining in 3107 working face, the microseismic event intensive area gradually develops from 17.35 m to high rock strata, and finally reaches 48.05 m. 3104 goaf roof caving zone, fractured zone height ; the position of the maximum settlement value is shifted from the middle of the 3107 goaf to the side of the 3104 goaf, and finally tends to be gentle in the middle of the 3106 goaf, and the position of the maximum settlement value of the strike side line gradually shifts to the side of the 2201 goaf. The research results can provide reference for the safe and efficient mining of coal resources and have important engineering practical significance.

Keywords : coal resources ; large mined-out area ; microseism ; overburden strata ; ground surface subsidence ; secondary activation

1. Introduction

As a crucial energy resource in China, coal plays a fundamental role in the nation's energy infrastructure. The extensive mining activities have led to widespread coal mining subsidence areas across the country[1-3] , which are frequently associated with surface collapse[4, 5] , ground fissures[6] , and soil degradation [7] . To address the challenges of resource extraction, the continuous small pillar mining method has been developed, which significantly enhances the recovery rate of coal resources, reduces the per-ton cost of coal extraction, extends the operational lifespan of mines, and mitigates the risk of mine pressure-related incidents[8, 9]. Nonetheless, this method results in the formation of extensive continuous goaf areas, complicating the movement characteristics of the roof strata within these zones[10]. In response to these challenges, Mu Zonglong et al. [11] used theoretical analysis, UDEC numerical simulation and industrial experiments to study the dynamic behavior of heavy layers and the mechanism of mining-induced earthquake-triggered surface damage. Gao Fuqaing et al. [12] used both the physical model and the numerical model successfully captured weighting as the longwall face advances. It is found that the periodic weighting not only involves the local direct roof and main roof of the cantilever beam behind the longwall working face, but also may involve the fracture of the rock bridge in the overburden above the fault zone. Hu Qingfeng et al. [13]established the subsidence coefficient model of overlying strata, and proposed a dynamic prediction model for predicting the movement and deformation of overburden caused by mining,

which can realize the dynamic quantitative prediction of overburden behavior. Tajdus Krzysztof [14] studied the settlement measured after the end of mining. The analysis shows that this process can last for months to decades or even hundreds of years, and the final surface settlement is still unclear. It depends on the individual characteristics of the mining medium, mining depth, mining system, the behavior of the surrounding rock and so on. Based on Volasov thick plate and moment tensor inversion theory, Zhang et al. [15]analyzed the fracture migration characteristics of hard rock and thick rock and the focal mechanism of mining-induced earthquakes. By analyzing the focal mechanism of mining-induced earthquakes, it has a certain guiding role in explaining the mechanism of mining-induced earthquakes.

In summary, current research on roof movement patterns and surface subsidence characteristics in large-scale mining areas under continuous small coal pillar conditions remains limited. Previous studies mainly focused on the movement of overlying strata in overlying strata structure, the research on the movement law of overlying strata in large goaf is limited, especially from the perspective of 3DEC numerical simulation. To address this research gap, this study focuses on the 11-3 104, 11-3 106, and 11-3 107 working faces of the Menkeqing Mine as a case study. Utilizing field microseismic monitoring data and surface subsidence measurements, combined with 3DEC numerical simulation technology, this paper systematically investigates the roof movement mechanisms and surface subsidence behavior in large-scale goaf areas under continuous small coal pillar mining conditions. The findings of this research are expected to provide valuable theoretical insights for roof management strategies in extensive goaf areas under similar mining conditions.

2. Engineering Geology Overview

The Menkeqing Coal Mine, a primary production site of Zhongtian Hechuang Energy Co., Ltd., boasts a designed annual production capacity of 8 million tons. The current focus of extraction is the No. 3-1 coal seam, which is situated at an average depth of 685 meters with a dip angle ranging from 1 to 3 degrees. This seam has an average thickness of 4.41 meters and is overlain by a 5.26-meter-thick siltstone layer serving as the immediate roof. The main roof, located at a distance of 5.26 to 72.76 meters above the No. 3-1 seam, predominantly consists of medium-grained sandstone. Currently, the mine is operating the 3-107 fully mechanized longwall face. Notably, the 3-106 working face (previously mined) and the 3-107 working face are positioned on either side of the 3-104 working face (also previously mined). Each of these working faces utilizes a narrow coal pillar (6 meters in width) for the layout of the gate roads in the mining system. With the rapid advancement of high-intensity, large-scale mining operations, the area of the mining zone has expanded significantly. The 3-107 mining area has merged with the previously developed 3-104 and 3-106 mining areas, forming an extensive mining zone approximately 1,000 meters in width and 3,000 meters in length (hereafter referred to as the large-scale mining area). The specific engineering layout is illustrated in Figure 1.

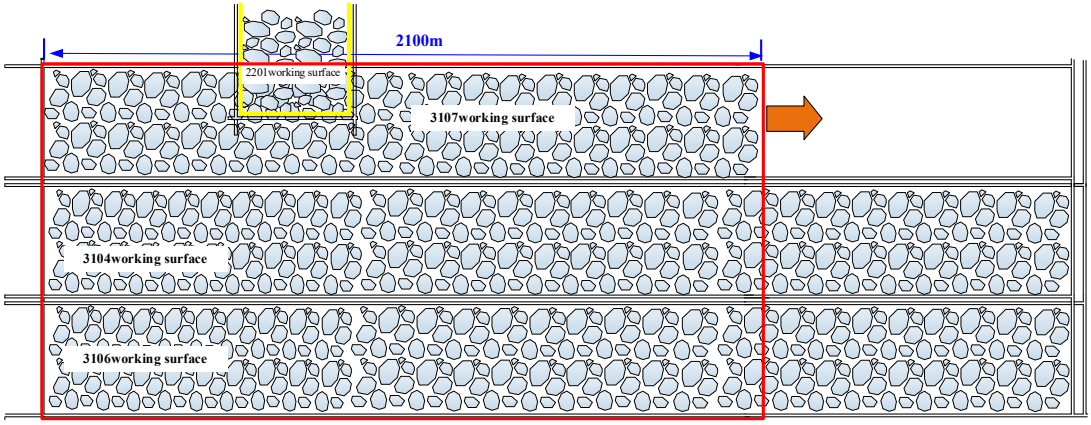


Fig.1 Engineering plane diagram

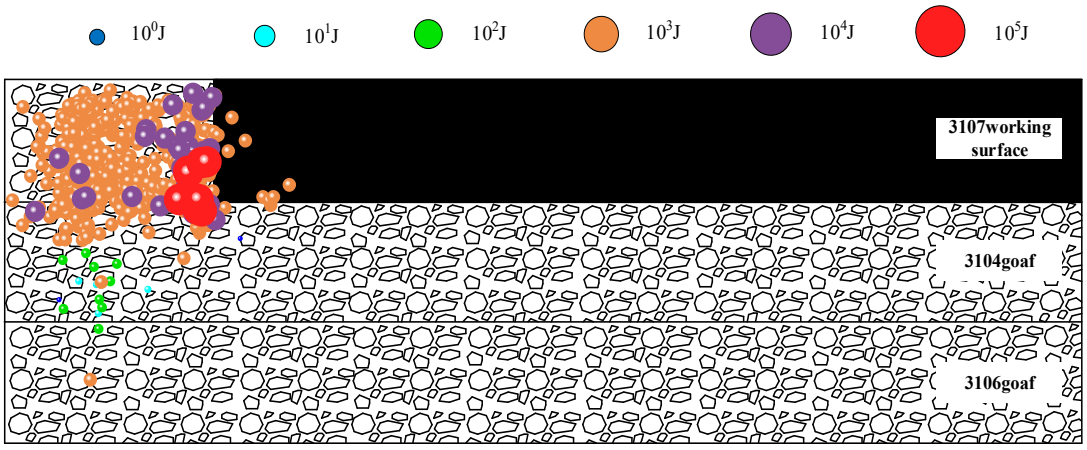
3. Characteristics of Microseismic Activity in Large-Scale Goaf Areas under Continuous Small Coal Pillar Mining Conditions

Microseismic monitoring technology represents a sophisticated approach for assessing rock mass stability through the detection and analysis of micro-vibration signals generated during stress-induced deformation and fracturing of rock formations or subsurface structures[16-18]. By systematically analyzing the spatial and temporal distribution, energy release patterns, and frequency characteristics of mining-induced seismic events, this method enables the comprehensive evaluation of structural damage mechanisms in overlying rock strata resulting from mining activities.

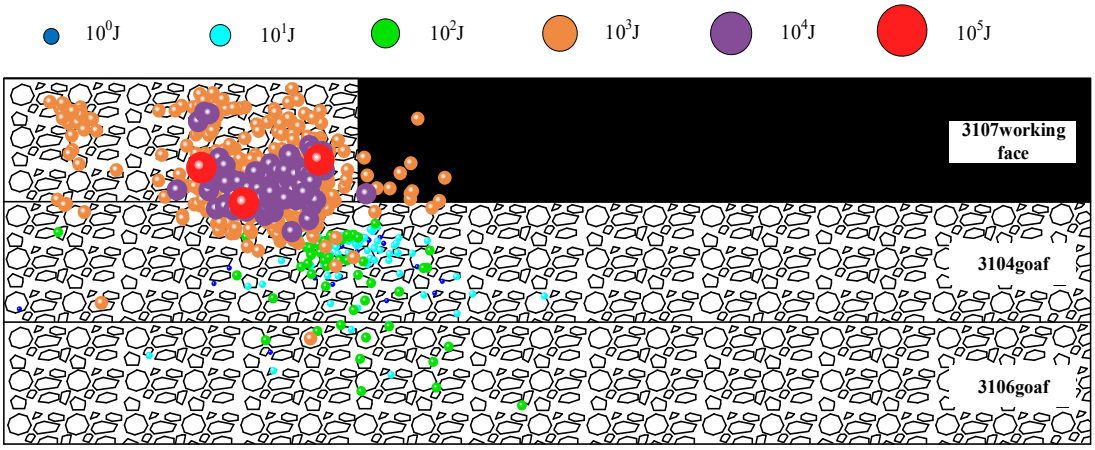
3.1 Temporal-Spatial Evolution Characteristics of Roof Activity during Working Face Advancement

Based on the spatial distribution and energy magnitude analysis of microseismic events, we systematically investigated the overburden rock response above the 3-104 and 3-106 working faces during the advancement of the 3-107 face. For this analysis, microseismic events occurring within 2,100 meters of the 3-107 face advancement were selected and spatially projected, as illustrated in Figure 2.

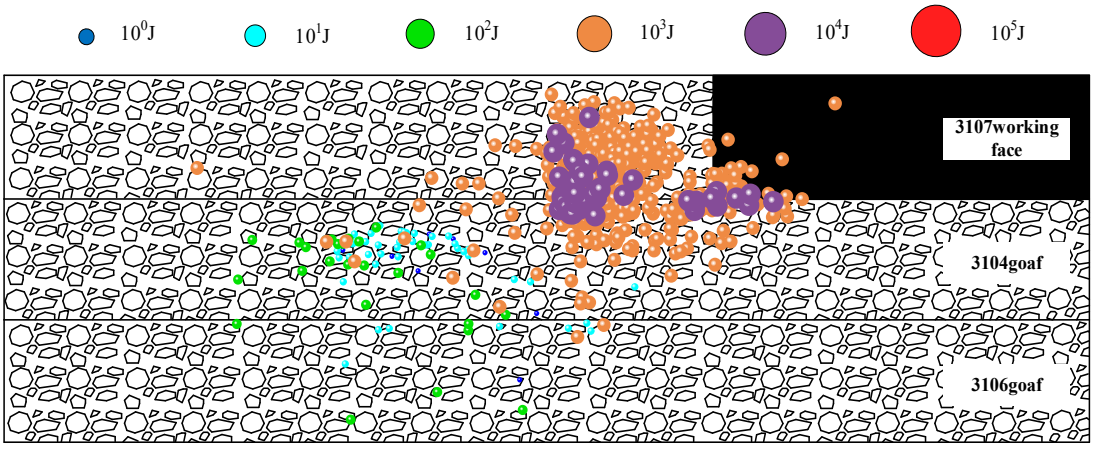
According to A. J. Mendecki, the energy classification standard of mining microseismic is proposed for the first time. 10^0 J $\leqslant$ E < 10^2 J is called low energy microseismic event, 10^2 J $\leqslant$ E < 10^4 J is called medium energy microseismic event, and E $\geqslant$ 10^5 J is called high energy microseismic event. According to the actual situation of Menkeqing, the deformation degree of roadway and roof in 10^0 J $\leqslant$ E < 10^4 J microseismic event area is small, 10^4 J $\leqslant$ E < 10^5 J is larger, and the deformation is the largest when E $\geqslant$ 10^5 J.Therefore, E $\geqslant$ 10^5 J is called high energy microseismic event, 10^4 J $\leqslant$ E < 10^5 J is called medium and high energy microseismic event, and 10^0 J $\leqslant$ E < 10^4 J is called small energy microseismic event.



(a) 3107 working face advancing to 500 m



(b) 3107 working face advancing to 1000 m



(c) 3107 working face advancing to 2100 m

Fig.2 Plane diagram of microseismic event distribution in large goaf

As illustrated in Figure 2(a), the analysis reveals distinct patterns of microseismic activity across the study area. High-energy microseismic events ($E \geq 10^5$ J) were recorded twice in the overburden strata above the 3-107 working face and three times at the junction between the 3-107 and 3-104 working faces. Notably, no high-energy events were detected in the overburden above the 3-106 working face. Medium-energy events (10^4 J $\leq E < 10^5$ J) were predominantly concentrated in the overburden above the 3-107 working face. Low-energy microseismic activity (10^0 J $\leq E < 10^4$

J) was primarily observed in the overburden above the 3-104 working face, while the 3-106 working face exhibited minimal microseismic activity. These observations demonstrate that when the 3-107 working face had advanced 500 meters, its mining operations exerted negligible influence on the overburden strata above the 3-106 working face. Furthermore, the impact on the overburden above the 3-104 working face was limited to the generation of a small number of low-energy microseismic events.

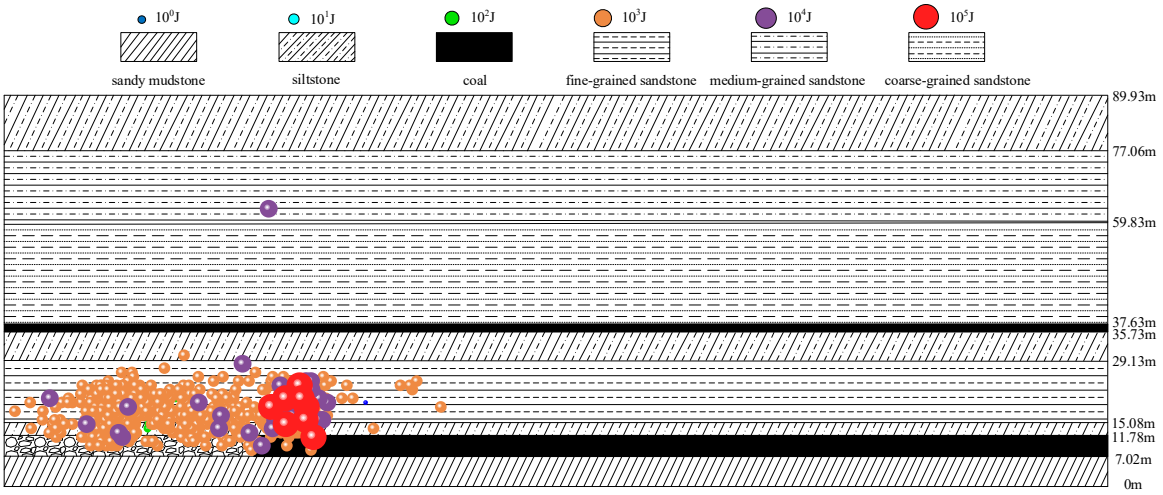
As demonstrated in Figure 2(b), the microseismic activity distribution reveals significant spatial variations. High-energy microseismic events ($E \geq 10^5$ J) were recorded twice in the overburden strata above the 3-107 working face and once at the interface between the 3-107 and 3-104 working faces. Medium-energy events (10^4 J $\leq E < 10^5$ J) were predominantly concentrated in the overburden above the 3-107 working face, while the overburden above the 3-106 working face exhibited minimal medium-energy activity. Low-energy microseismic events (10^0 J $\leq E < 10^4$ J) were primarily distributed in the overburden above the 3-104 working face, with a minor portion occurring above the 3-106 working face.When the 3-107 working face had advanced to 1,000 meters, the frequency of medium- and low-energy microseismic events in the overburden above the 3-104 working face showed a gradual increase. Concurrently, a limited number of low-energy microseismic events began to emerge in the overburden above the 3-106 working face, indicating an extended influence range of mining activities.

As evidenced in Figure 2(c), the distribution of microseismic activity demonstrates distinct spatial patterns. Medium- to high-energy microseismic events (10^4 J $\leq E < 10^5$ J) were predominantly concentrated in the overburden strata above the 3-107 working face, with a limited number occurring above the 3-104 working face. Notably, two medium- to high-energy events were also detected in the overburden above the 3-106 working face. Low-energy microseismic events (10^0 J $\leq E < 10^4$ J) were primarily observed in the overburden above the 3-104 working face. Comparative analysis reveals a progressive increase in the frequency of medium- and low-energy microseismic events in the overburden above the 3-104 working face compared to previous mining stages. Additionally, a more pronounced occurrence of low-energy events was observed in the overburden above the 3-106 working face. These phenomena can be attributed to the expanding mining scope and intensifying extraction activities at the 3-107 working face. The implementation of continuous small pillar mining significantly influences roof strata movement within the large goaf area, consequently inducing varying magnitudes of microseismic activity in the overburden of adjacent workings.

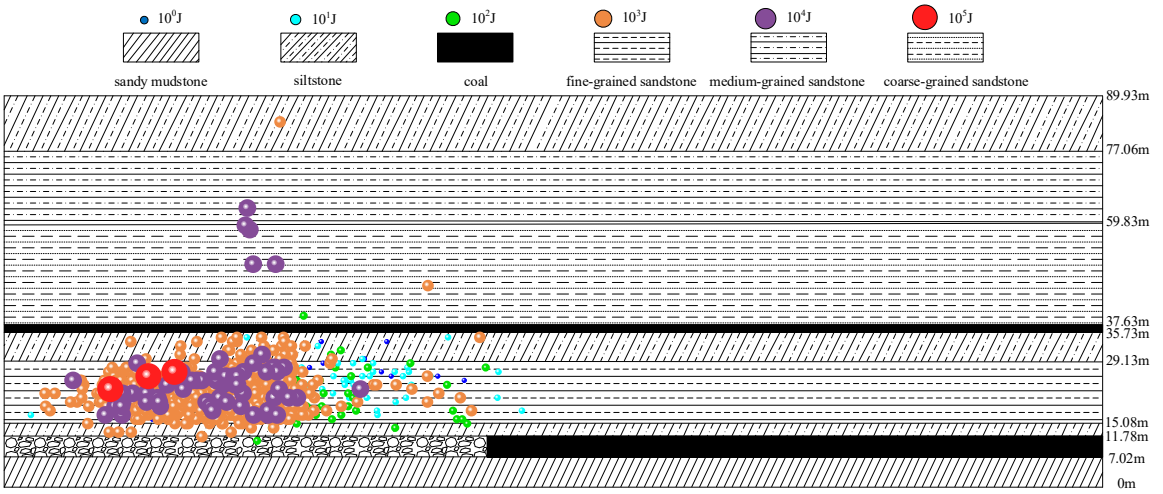
In summary, the roof strata movement in the goaf area during the initial mining stage of the 3-107 working face exhibited minimal influence on adjacent workings. However, as the mining face advanced and approached completion, the roof movement in the goaf area progressively impacted neighboring workings, leading to additional damage to the overlying strata above adjacent faces. Notably, the rock strata above the 3-106 working face remained relatively unaffected throughout the mining process.

3.2 Vertical Displacement Characteristics of Roof Strata in Mining-Induced Goaf Areas

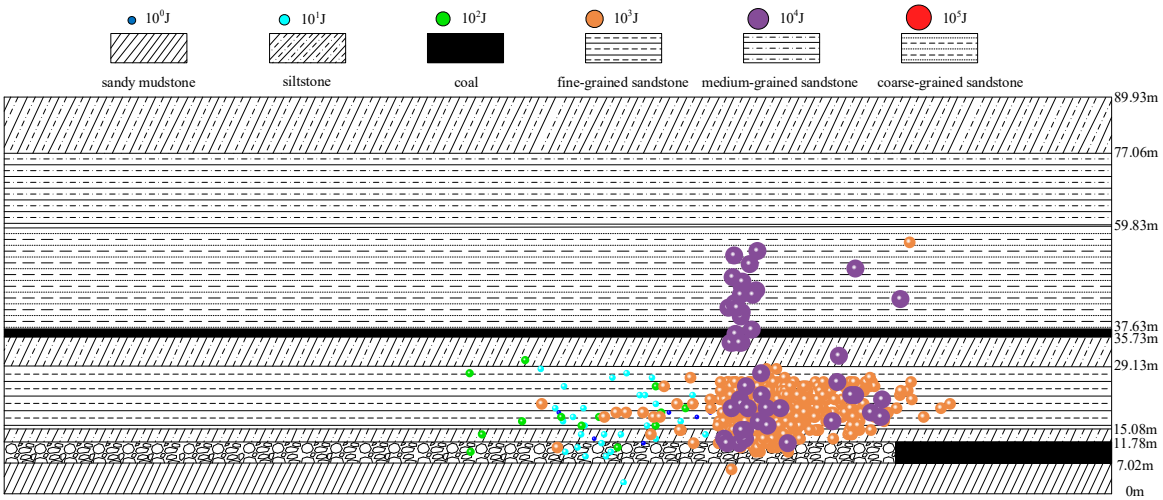
Based on the spatial distribution and energy magnitude of microseismic events, we systematically investigated the impacts on overlying strata above the 3-104 and 3-106 working faces during the advancement of the 3-107 face. Microseismic events occurring within a 2,100-meter range of the 3-107 face advancement were selected and projected along the mining direction, as illustrated in Figure 3.



(a) 3107 working face advancing to 500 m



(b) 3107 working face advancing to 1000 m



(c) 3107 working face advancing to 2100 m

Fig.3 Distribution profile of microseismic events in large goaf

As illustrated in Figure 3(a), microseismic events are predominantly concentrated in the lower strata of the roof rock layers. The majority of these events are distributed within the siltstone layer (0-3.3 m above the coal seam) and fine-grained sandstone layer (3.3-17.35 m above the coal seam).

A limited number of medium- to high-energy events are observed in the medium-grained sandstone layer at approximately 46.75 m above the coal seam. Figure 3(b) demonstrates that microseismic activity extends to both middle and lower roof strata. Low-energy events are primarily distributed within three distinct layers: the siltstone (0-3.3 m), fine-grained sandstone (3.3-17.35 m), and upper siltstone (17.35-29.35 m) above the coal seam. Medium- to high-energy events are mainly concentrated in the fine-grained sandstone layer (3.3-17.35 m above the coal seam). As shown in Figure 3(c), the microseismic event distribution shifts towards middle and upper roof strata. Low-energy events predominantly occur in the fine-grained sandstone and siltstone layers within 3.3-17.35 m above the coal seam, while medium- to high-energy events are primarily located in the fine-grained sandstone, coarse-grained sandstone, and medium-grained sandstone layers up to 44.59 m above the coal seam.

In summary, the evolutionary pattern of microseismic events demonstrates a distinct vertical progression. Initially, microseismic activity is predominantly concentrated in the lower strata, specifically within the siltstone and fine-grained sandstone layers located 0-17.35 meters above the roof of the 3-1 coal seam. As the 3-107 working face advances, the distribution of microseismic events evolves through three distinct phases:

Initial Stage: Microseismic events are primarily concentrated in the lower strata (0-17.35 m), particularly within the siltstone (0-3.3 m) and fine-grained sandstone (3.3-17.35 m) layers.

Intermediate Stage: During the mid-mining phase of the 3-107 working face, the microseismic activity zone extends upward to the siltstone layer at 17.35-29.35 meters above the coal seam.

Final Stage: At the completion of the 3-107 mining operations, the microseismic event concentration area further migrates to the coarse-grained sandstone layer at 29.35-48.05 meters above the coal seam.

4. Numerical analysis of subsidence in continuous small coal pillar mining in large open area

4.1 Numerical modeling

To investigate the development of rock fracturing and subsidence characteristics in the large-scale mining area, a comprehensive numerical simulation was conducted using 3DEC software. The model was designed to analyze overburden movement and surface subsidence patterns. The simulation incorporated three working faces (3-104, 3-106, and 3-107), each with a length of 320 meters. The study focused on roof collapse mechanisms in the 3-107 working face and adjacent mining areas during three distinct advancement stages: 500 meters, 1,000 meters, and 2,100 meters from the initial cut. The model configuration included 50-meter protective coal pillars on both the starting and stopping sides of the 3-107 working face. The final model dimensions were established as X × Y × Z = 1,100 m × 3,000 m × 167.5 m, where the X-axis represents the working face advancement direction and the Y-axis corresponds to the face inclination direction. For mesh generation, the model employed variable block sizes to optimize computational efficiency and accuracy: Upper rock layers: 40m × 10 m × 20 m; Lower rock layers: 40 m × 10 m × 35 m; Intermediate rock layers: 5 m × 10 m × 5 m . This refined mesh configuration allows for detailed analysis of stress distribution and deformation patterns throughout the overburden strata.

The numerical model was subjected to an equivalent vertical stress of 16.5 MPa at its upper boundary to simulate overburden pressure. The lateral pressure coefficient was set to 1.0, and gravitational acceleration was defined as 9.8 m/s². Boundary conditions were implemented as follows: horizontal displacements were constrained at the front and back boundaries, while both

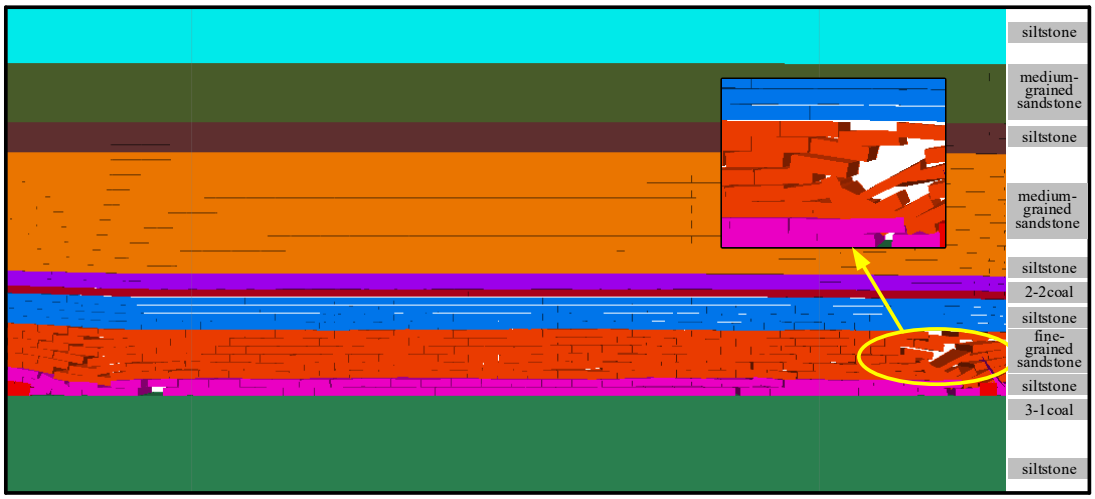
horizontal and vertical displacements were fixed at the lower boundary. The constitutive behavior of the rock mass was simulated using the Mohr-Coulomb failure criterion. The geomechanical properties of coal and rock strata, including density, elastic modulus, Poisson's ratio, cohesion, and internal friction angle, are detailed in Table 1.

Table 1 Physical and mechanical parameters of model formation lithology

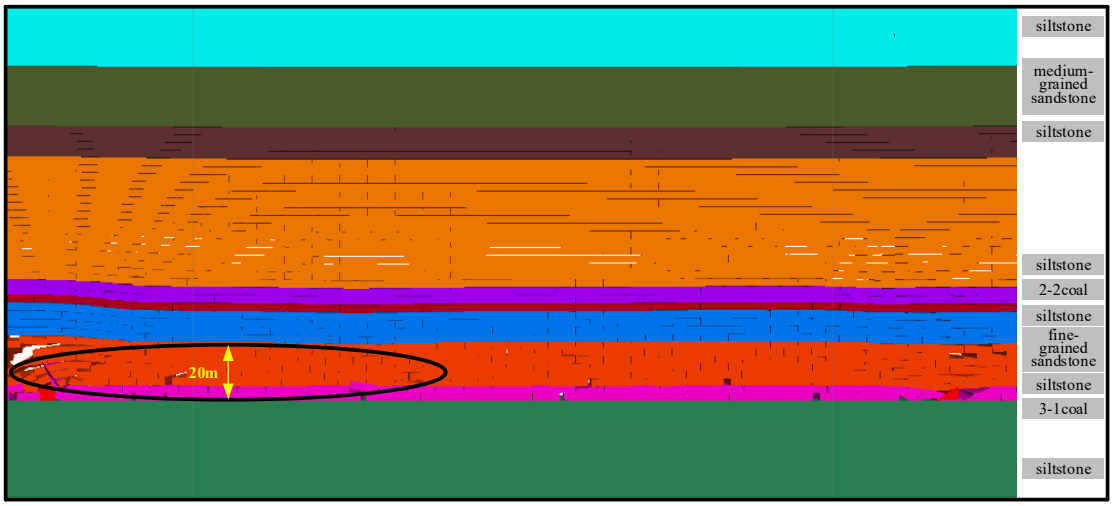
stratigraphic lithology	bulk /GPa	shear /GPa	density /（kg·m^{-3}）	friction /（°）	cohesion /MPa	tensile strength /MPa
siltstone	11.0	8.0	2 050	32.0	7.0	3.6
coal	2.0	1.5	1 300	19.4	3.0	1.2
fine sandstone	16.0	14.0	2 200	33.2	6.0	3.1
medium sandstone	8.0	7.0	2 100	30.0	6.3	3.2

4.2 Numerical simulation study and analysis of mining subsidence

The roof failure patterns were analyzed at three distinct advancement stages of the 3-107 working face: 500 meters, 1,000 meters, and 2,100 meters. Due to the minimal roof movement observed in the 3-106 mining area, the simulation results focus on the roof failure characteristics in the 3-104 and 3-107 mining areas. The corresponding roof breakage patterns are illustrated in Figures 4, 5, and 6, respectively.

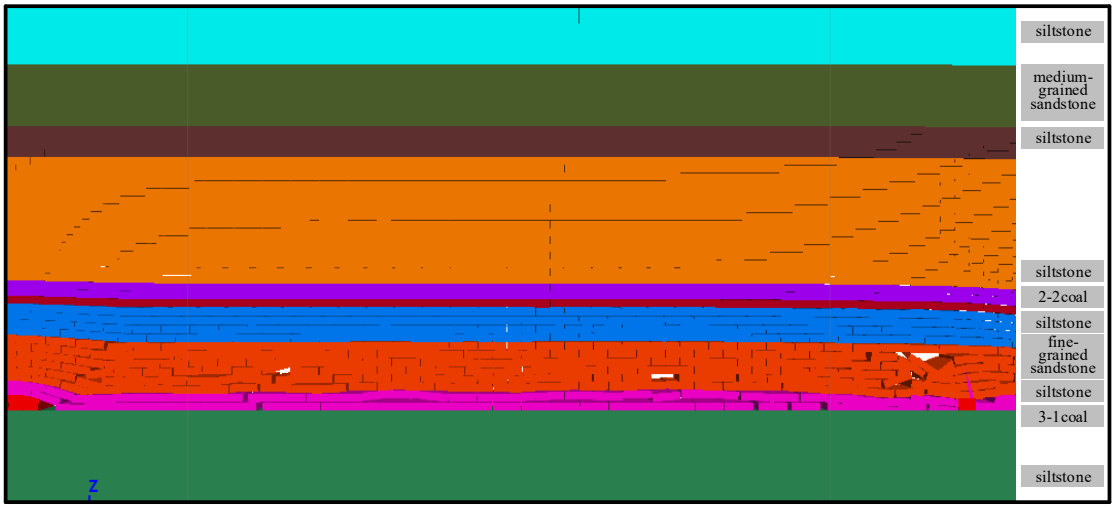


(a) 3 107 working face

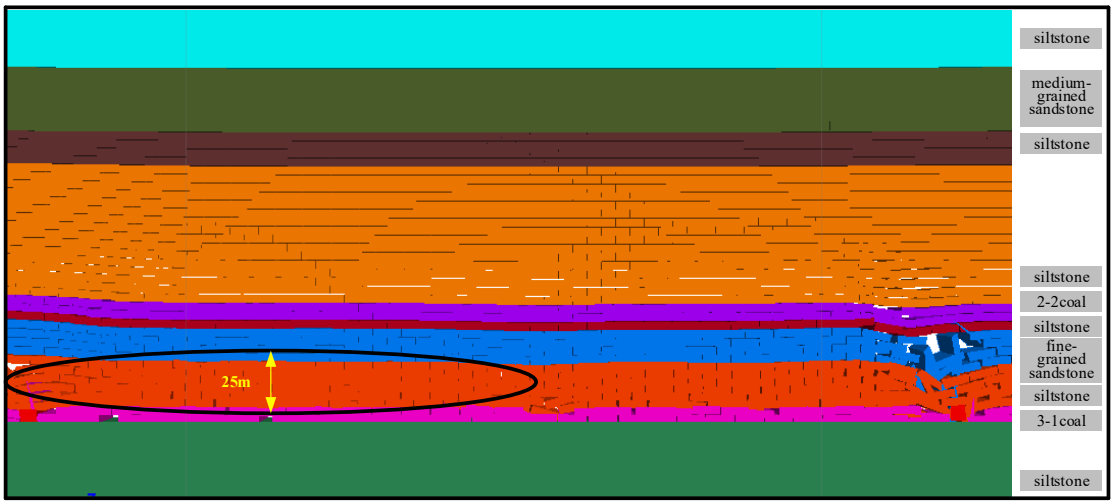


(b) 3 104 working face

Fig.4 The shape of roof overburden in different working faces when 3107 advances 500 m.

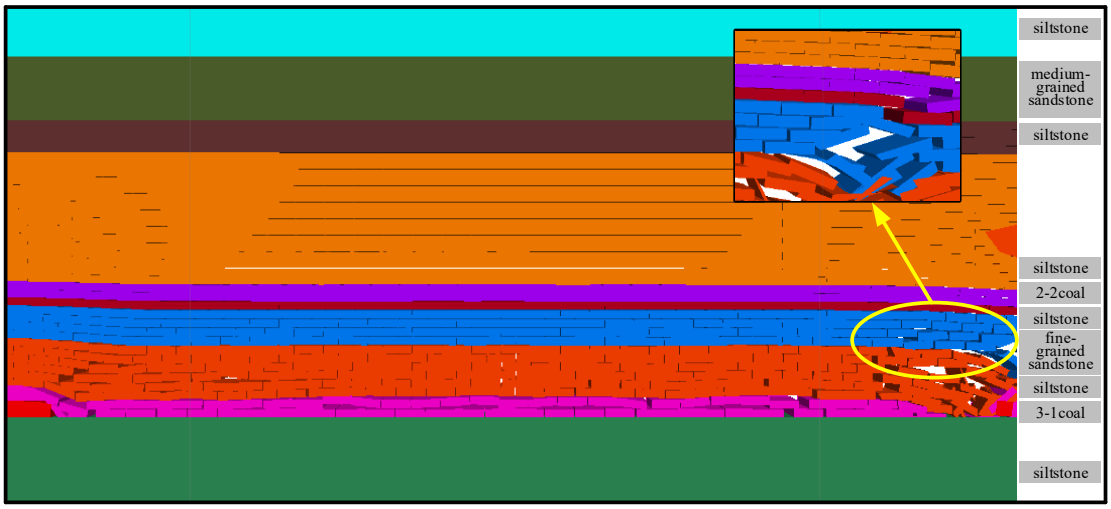


(a) 3 107 working face

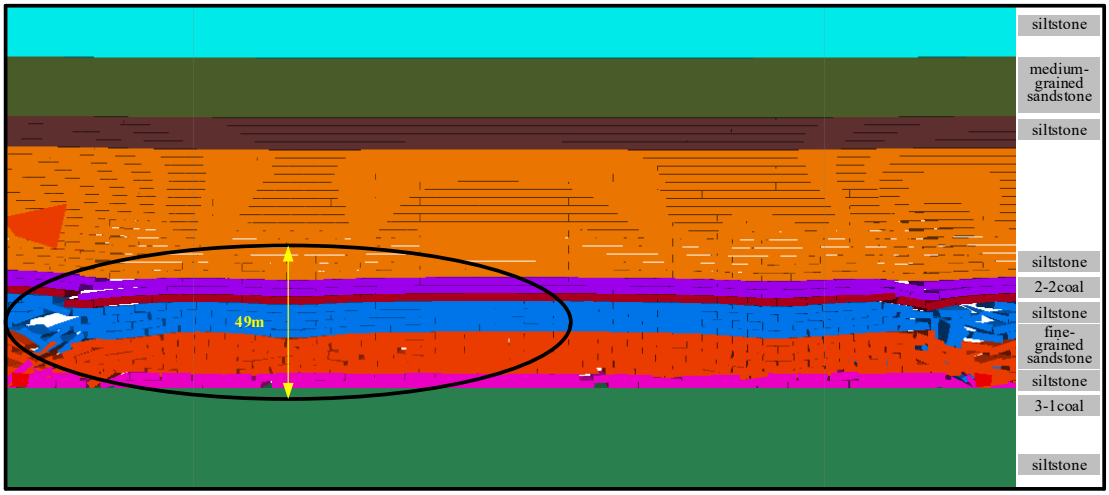


(b) 3 104 working face

Fig. 5 3107 Roof overburden morphology of different working faces when advancing 1 000 m.



(a) 3 107 working face



(b) 3 104 working face

Figure 6 3107 When advancing 2 100 m, the roof overburden morphology of different working faces is different.

Figure 4(a) illustrates the initial roof failure characteristics when the 3-107 working face has advanced 500 meters. The immediate roof above the 3-107 coal seam has collapsed, while the main roof remains intact, forming a voussoir beam structure. Partial fracturing is observed in the main roof at the junction between the 3-107 and 3-104 working faces. Figure 4(b) demonstrates that the collapsed zone above the 3-104 working face extends approximately 20 meters vertically. As shown in Figure 5(a), when the 3-107 working face reaches 1,000 meters of advancement, the main roof above the 3-107 coal seam maintains its structural integrity, and no additional damage is observed at the junction between the 3-107 and 3-104 working faces. Figure 5(b) reveals that the collapse height above the 3-104 working face has increased to approximately 25 meters. Figure 6(a) presents the roof conditions when the 3-107 working face has advanced 2,100 meters. The main roof above the 3-107 coal seam exhibits partial collapse, although the voussoir beam structure persists. Significant fracturing occurs in the main roof at the junction between the 3-107 and 3-104 working faces, with delamination cracks developing in the medium-grained sandstone layer. Figure 6(b) shows that the collapse height above the 3-104 working face has extended to approximately 49 meters, with multiple delamination cracks observed in the central portion of the medium-grained sandstone layer, indicating an expansion of the fractured zone. In the characteristics of microseismic activity, when 3107 is mined to 2100 m, the medium and high energy microseismic events are concentrated in the range of 44.59 m above the coal seam. The numerical simulation results are almost consistent with the actual microseismic monitoring results, and the conclusion is credible.

In summary, the progressive advancement of the 3-107 working face significantly influences the overlying strata dynamics. The rock strata above the 3-104 working face exhibit increasing damage intensity, manifested through three primary aspects:

1. Progressive elevation of roof collapse height in the 3-104 area;
2. Multiplication of delamination fractures within the large-scale goaf area
3. Vertical expansion of the fractured zone

5. Observations of surface settlement in large mining areas

The extensive extraction of coal resources from underground deposits has led to increasingly significant challenges associated with surface subsidence and mining-induced damage. Mining subsidence not only disrupts the ecological balance of mining areas but also causes substantial

damage to surface structures and infrastructure [19, 20] . To mitigate these impacts, it is essential to develop protective measures for surface structures, minimizing their exposure to mining-related damage while simultaneously optimizing underground coal resource recover [21, 22] . These objectives necessitate comprehensive research into the patterns and mechanisms of surface movement and deformation resulting from underground mining activities.

5.1 Layout of survey lines and time of testing

To investigate surface subsidence patterns in large-scale goaf areas under continuous small coal pillar mining conditions, a comprehensive monitoring network was established. The network consists of two strike-oriented monitoring lines (Line A and Line E) and two dip-oriented monitoring lines (Line C and Line D), as illustrated in Figure 8. The dip-oriented monitoring lines (C and D) span approximately 1,500 meters with an inter-line spacing of 300 meters. These lines originate from the centerline of the 3-106 working face, extending northward to cover an additional 550 meters beyond the 3-107 working face boundary. The strike-oriented Line E follows the centerline of the 3-104 working face, extending 550 meters in length. Its western starting point is positioned 150 meters west of Line C, while its eastern terminus lies 100 meters east of Line D. Line A, another strike-oriented monitoring line, is aligned with the centerline of the 3-107 working face. This 700-meter-long line begins 200 meters west of Line C and terminates approximately 200 meters east of Line D. The monitoring points along each survey line were strategically positioned at 25-35 meter intervals, determined by surface conditions, resulting in a total of 168 monitoring stations across the network.

The monitoring program was conducted over a nine-month period from October 20, 2023, to July 20, 2024, during which 23 comprehensive monitoring sessions were completed. Table 2 presents the detailed temporal correspondence between each monitoring session and the advancement progress of the 3-107 working face, providing a chronological framework for analyzing surface subsidence development in relation to mining activities.

Table 2 Subsidence detection time and working face advancing distance

Frequency of monitoring	Monitoring time	Propulsion distance	Frequency of monitoring	Monitoring time	Propulsion distance
1	2 023.10.20	579.4 m	13	2 024.03.28	1 417.4 m
2	2 023.11.08	708.9 m	14	2 024.04.04	1 458.6 m
3	2 023.11.23	762.5 m	15	2 024.04.15	1 511.0 m
4	2 023.12.15	819.1 m	16	2 024.04.24	1 563.8 m
5	2 023.12.22	853.5 m	17	2 024.04.30	1 592.6 m
6	2 023.12.29	873.0 m	18	2 024.05.07	1 637.4 m
7	2 024.01.15	965.2 m	19	2 024.05.23	1 782.6 m
8	2 024.01.31	1 074.6 m	20	2 024.06.05	1 823.8 m
9	2 024.02.27	1 230.6 m	21	2 024.06.20	1 852.9 m
10	2 024.03.05	1 275.2 m	22	2 024.07.10	1 973.4 m

11	2 024.03.14	1 329.8 m	23	2 024.07.20	2 087.0 m
12	2 024.03.20	1 359.0 m			

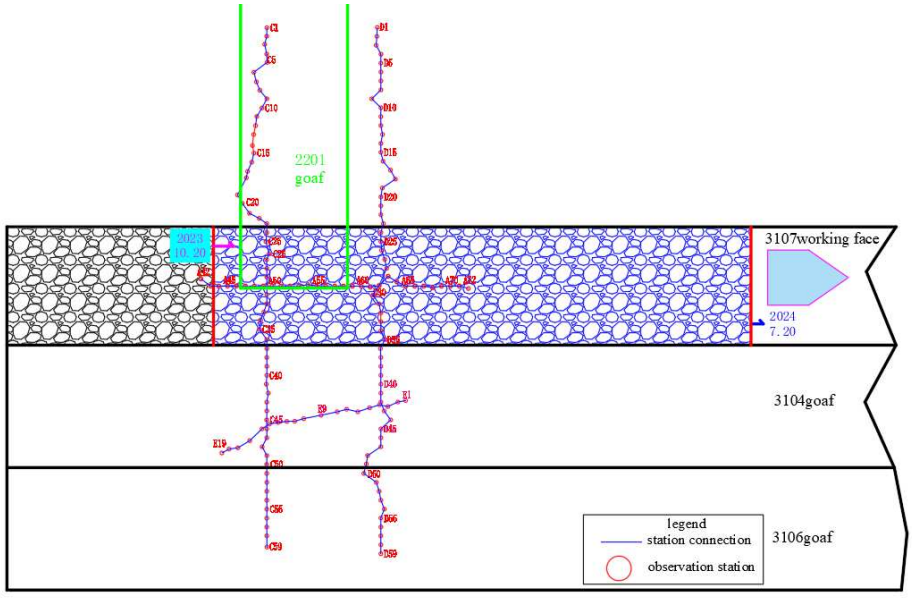


Fig. 7 Location distribution of measuring points

5.2 11-3 107 Workings Mining Surface Subsidence Patterns

The monitoring results revealed surface rock movement patterns in the large mining area influenced by the 3-107 working face. Figure 8 illustrates the dynamic evolution of topographic relief, while Figure 9 quantifies relative displacement changes. Specifically:

1. Figure 8(a) displays the initial topographic relief derived from the first monitoring dataset;

2. Figures 8(b1-b22) sequentially document elevation variations from the second to twenty-third measurements, calculated relative to the baseline;

3. Figure 8(c) presents the final relief configuration based on the twenty-third (terminal) monitoring dataset.

The three-dimensional model in Figure 8 was delineated by survey lines A, C, D, and E, forming a rectangular boundary that encompasses the critical deformation zone.

Figure 8 provides a comprehensive visualization of surface subsidence patterns in the large-scale goaf area during the mining of the 3-107 working face. The analysis reveals several key observations:

1.Temporal Evolution of Subsidence:

From October 20, 2023 (advancement: 579.4 m) to July 20, 2024 (advancement: 2,087.0 m)；Progressive expansion of the surface subsidence basin;Continuous increase in maximum subsidence values.

2. Spatial Distribution Characteristics:

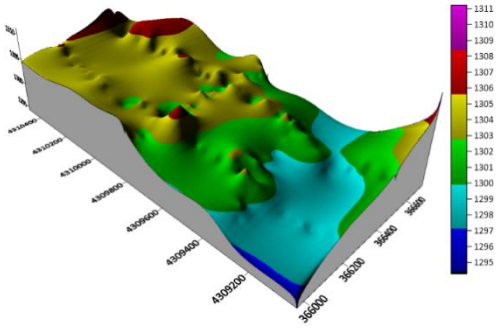
The point of maximum subsidence gradually migrates toward the goaf area; Subsidence intensity decreases progressively toward the southern regions; Most pronounced subsidence observed near the 3-107 working face.

3. Boundary Conditions:

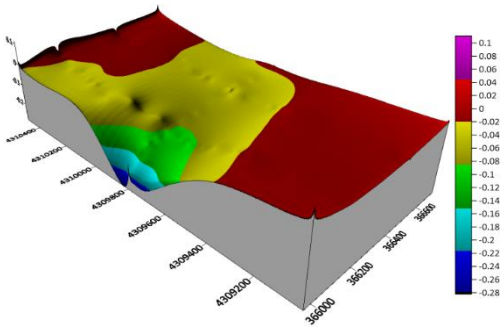
Southern boundary defined by measurement points C59 and D59; Initial signs of subsidence development in the central 3-106 mining area; No significant subsidence increase observed in

southernmost regions.

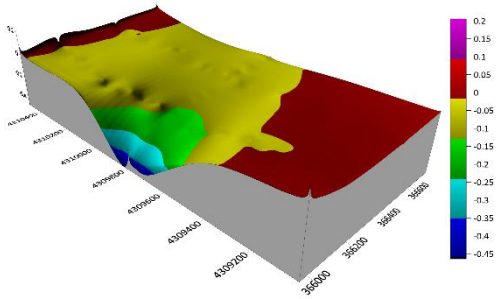
These findings demonstrate the dynamic nature of surface deformation in response to progressive mining activities, with distinct spatial and temporal patterns of subsidence development.



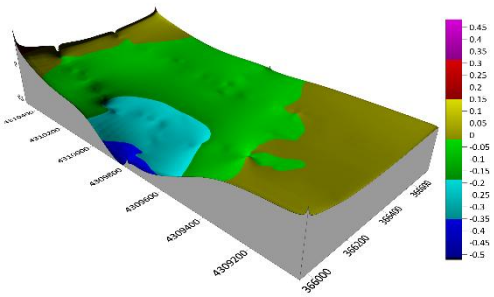
(a) Terrain-first measurement



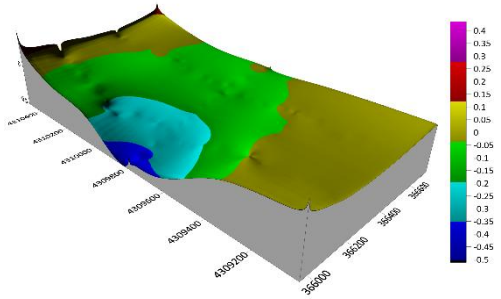
(b1) Relative variation of the first settlement



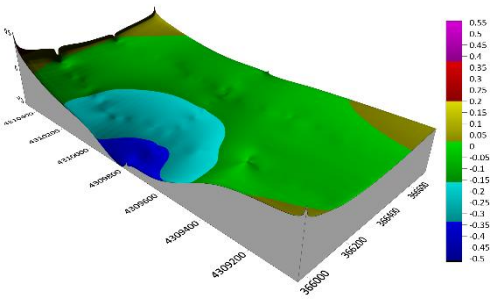
(b2) Relative variation of the second settlement



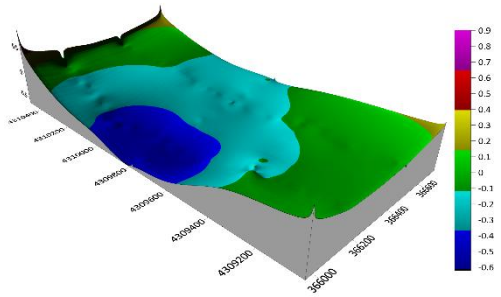
(b3) Relative variation of the third settlement



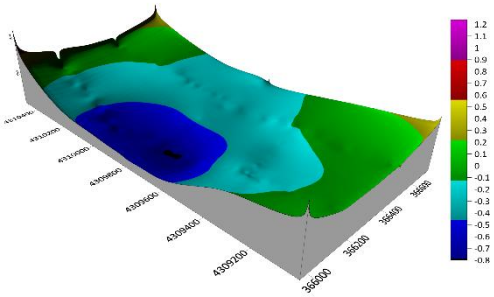
(b4) Relative variation of the fourth settlement



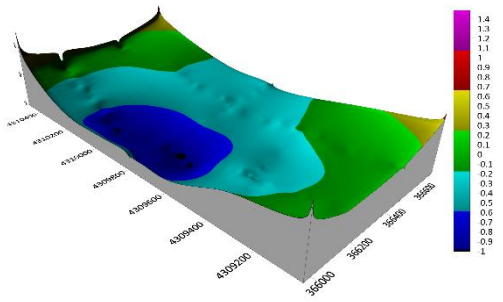
(b5) Relative variation of the fifth settlement



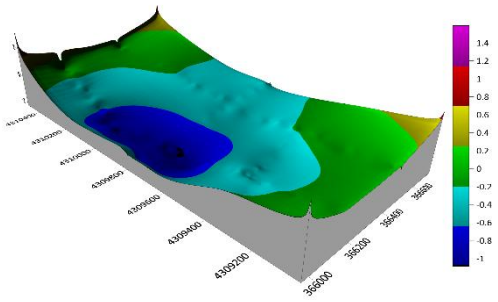
(b6) Relative variation of the sixth settlement



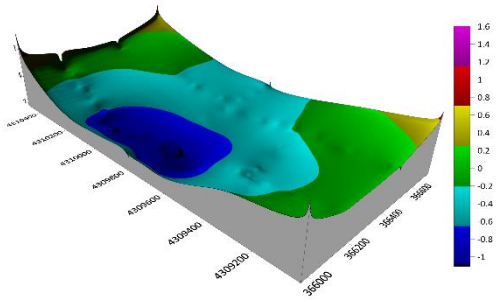
(b7) Relative variation of the seventh settlement



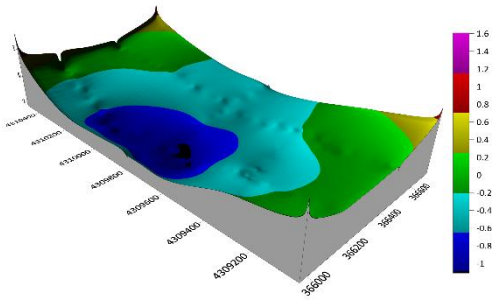
(b8) The relative variation of the eighth settlement



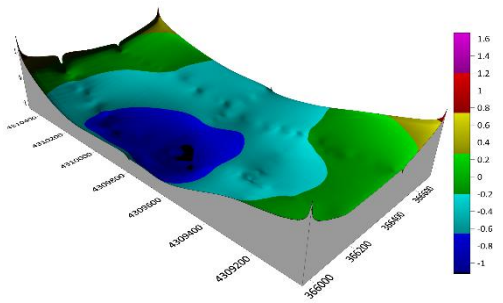
(b9) Relative variation of the ninth settlement



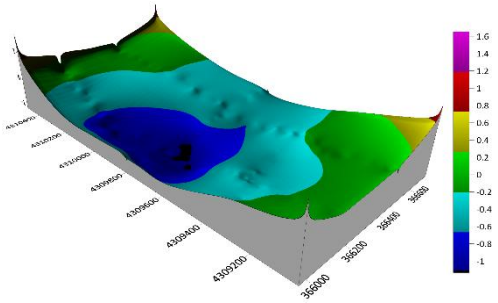
(b10) Relative variation of the tenth settlement



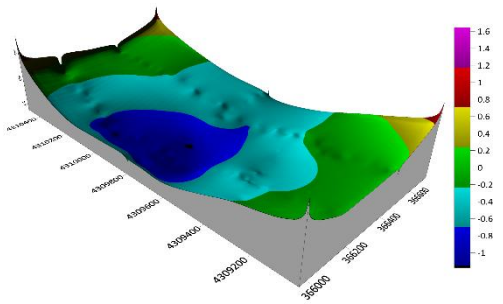
(b11) Relative variation of the eleventh settlement



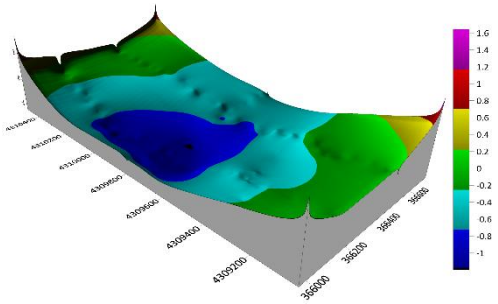
(b12) Relative variation of the twelfth settlement



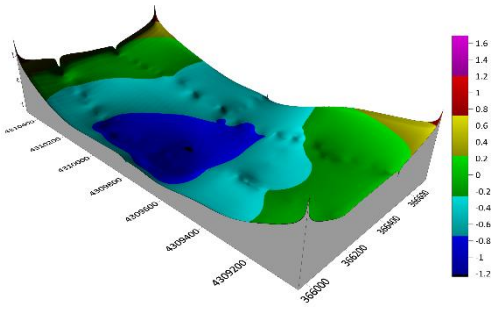
(b13) Relative variation of the thirteenth settlement



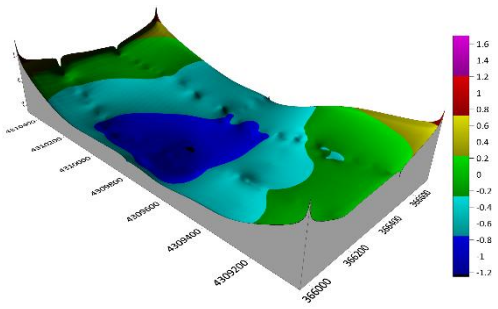
(b14) Relative variation of the fourteenth settlement



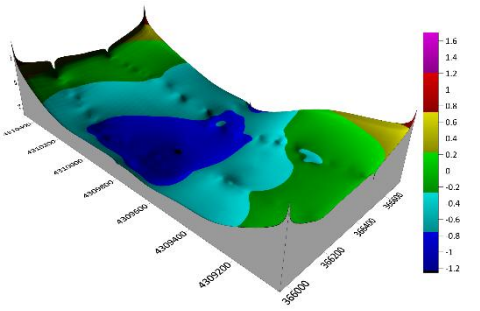
(b15) Relative variation of the fifteenth settlement



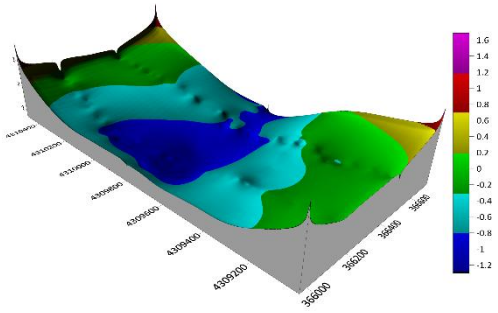
(b16) Relative variation of sixteenth settlement



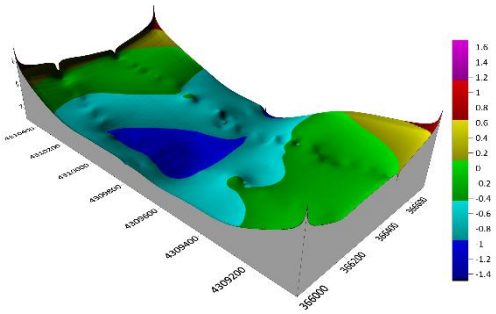
(b17) Relative variation of the seventeenth settlement



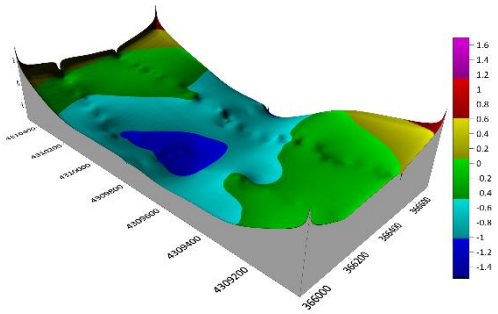
(b18) The relative variation of eighteenth settlement



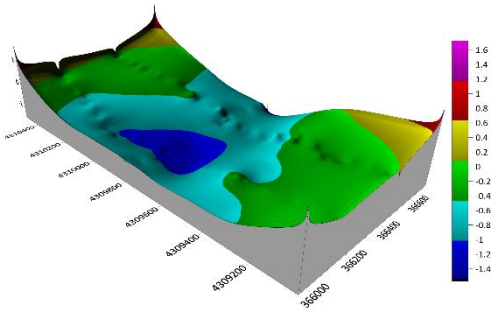
(b19) The relative variation of nineteenth settlement



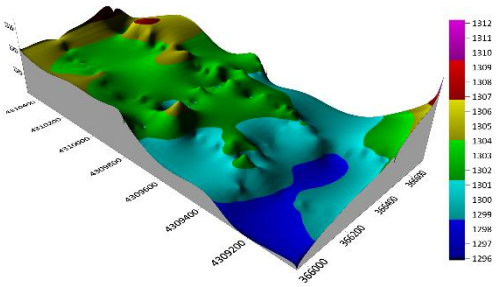
(b20) The relative variation of the twentieth settlement



(b21) Relative variation of the twenty-first settlement

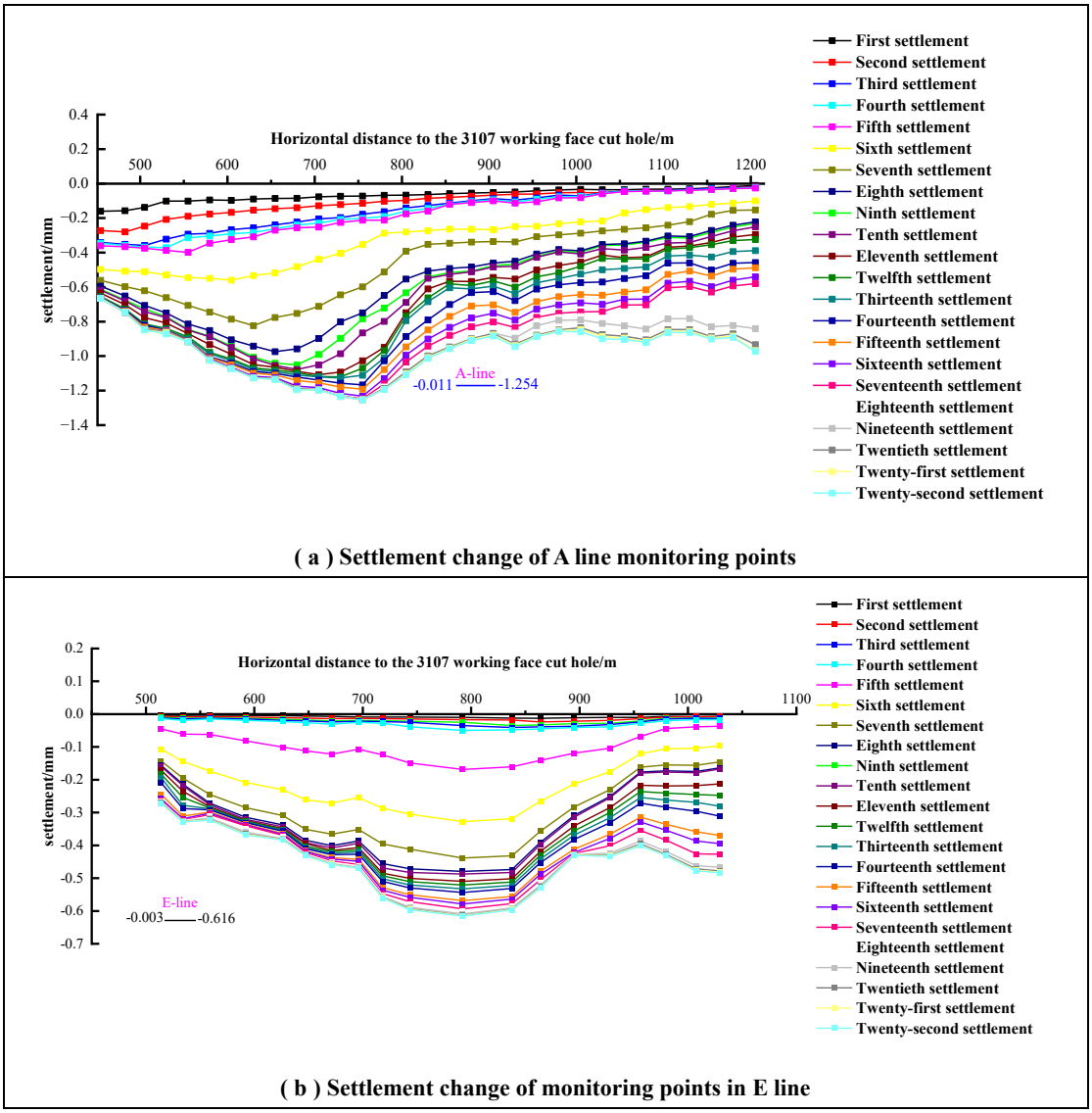


(b22) Relative variation of twenty-second settlement



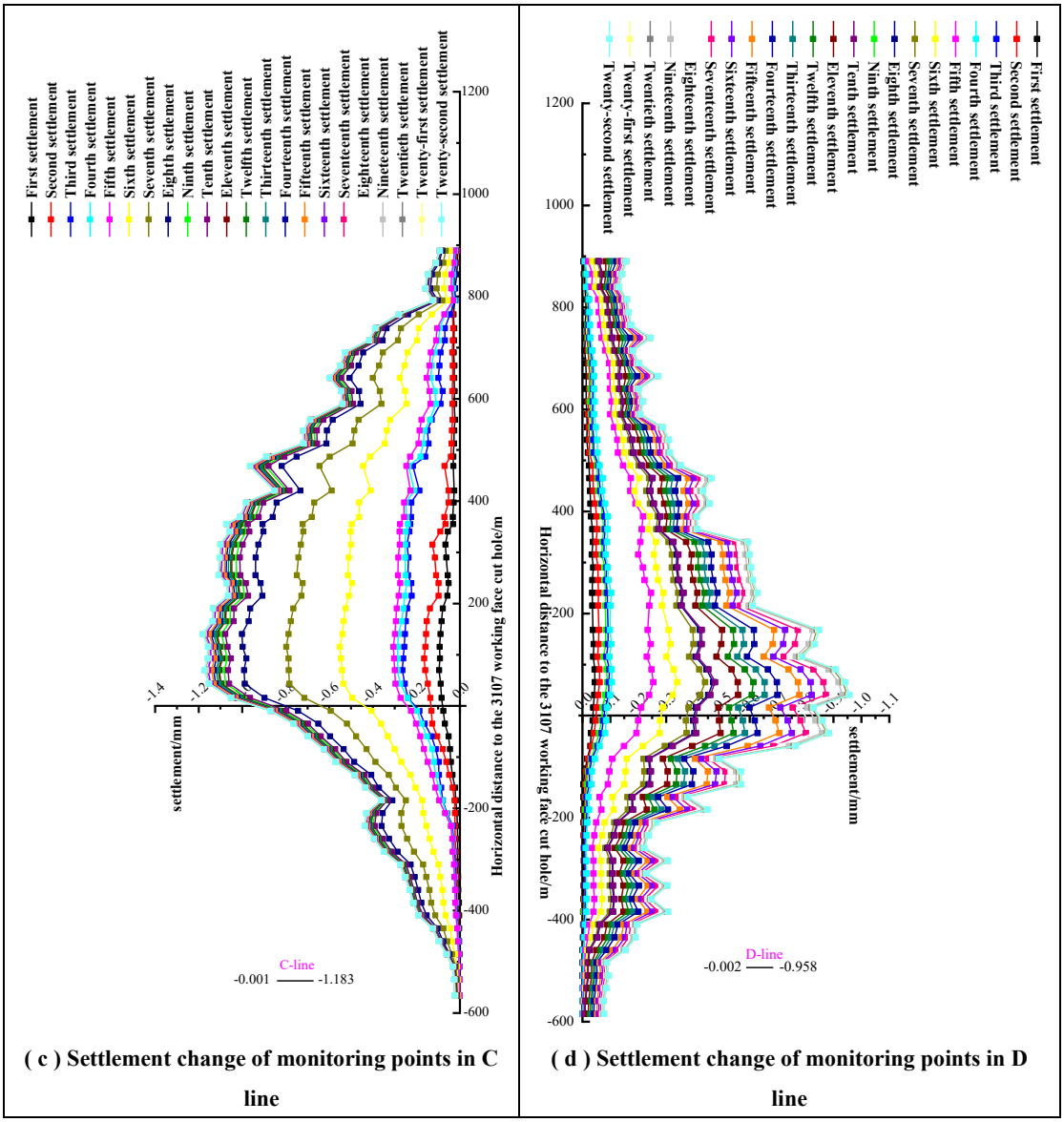
(c) Terrain-final measurement

Figure 8 3107 working face mining under the influence of large goaf surface rock movement change figure



(a) Settlement change of A line monitoring points

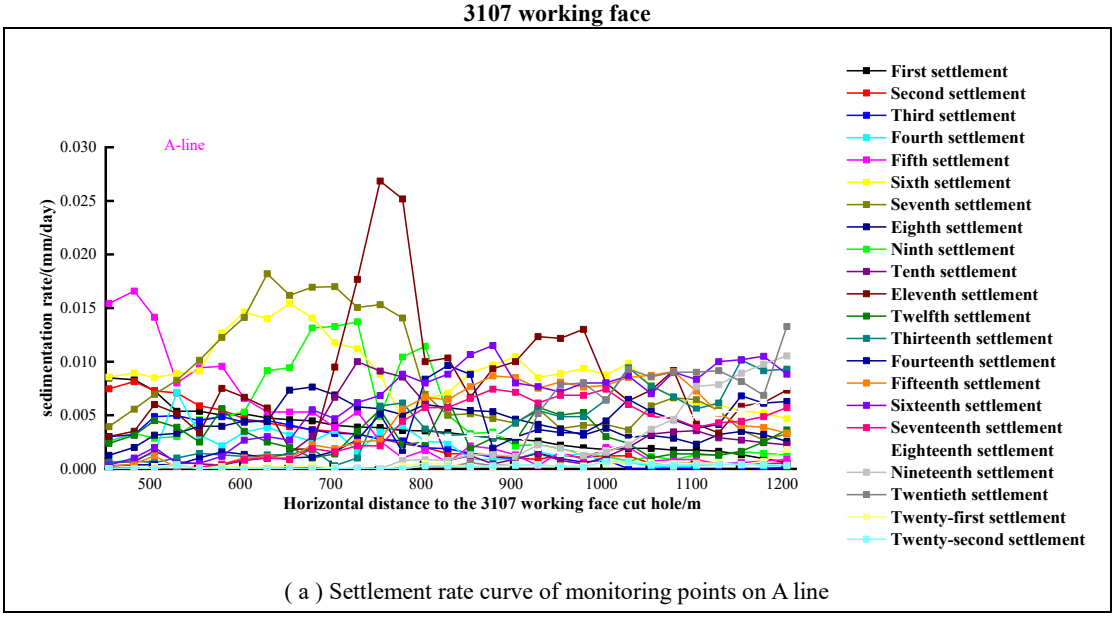
(b) Settlement change of monitoring points in E line



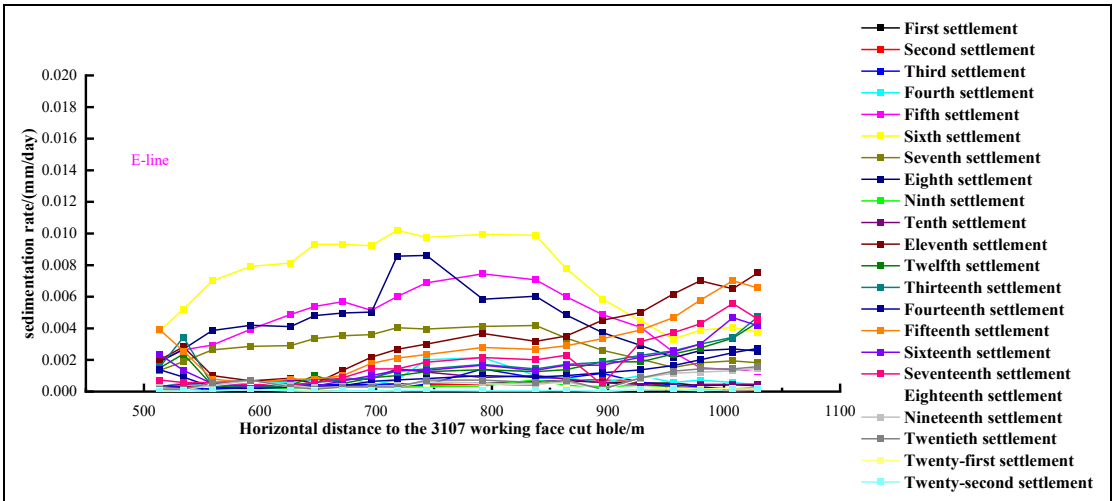
(c) Settlement change of monitoring points in C line

(d) Settlement change of monitoring points in D line

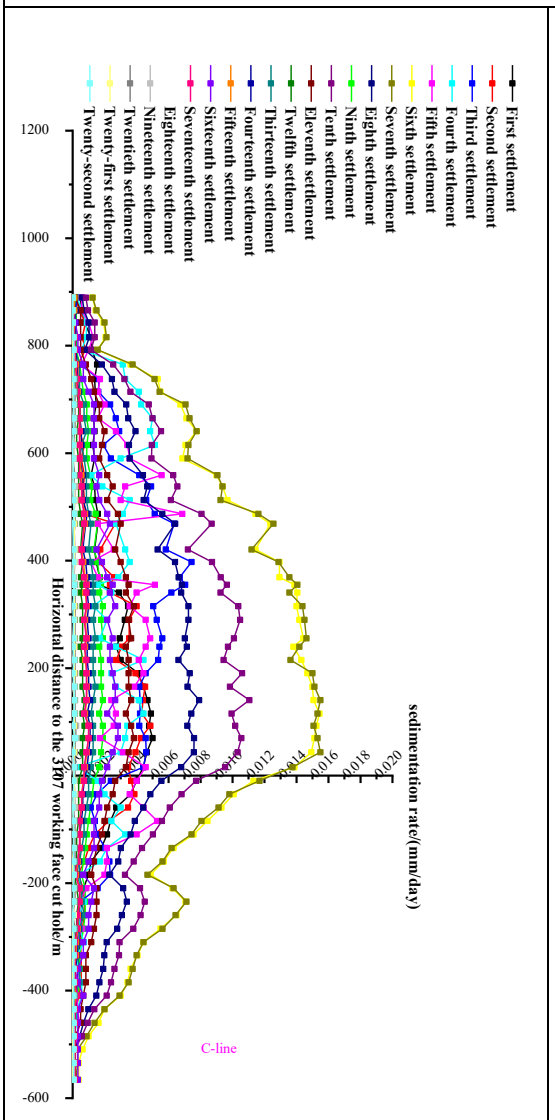
Fig. 9 Curve of change of surface rock movement in the large hollow area under the influence of mining in 3107 working face



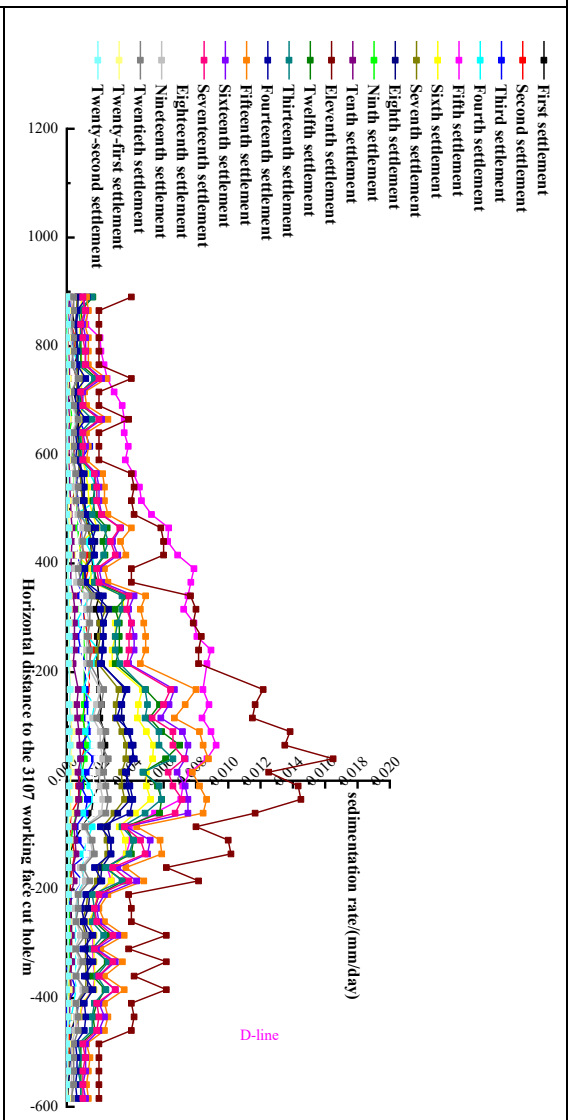
(a) Settlement rate curve of monitoring points on A line



(b) Settlement rate curve of monitoring points on E line



(c) Settlement rate curve of monitoring points on C line



(d) Settlement rate curve of monitoring points on D line

Figure 10 The subsidence rate curve of surface rock movement in large goaf under the influence of mining in 3107 working face

To quantitatively analyze the subsidence patterns, the relative subsidence changes at monitoring points under the influence of the 3-107 working face mining operations were plotted, as shown in Figures 9(a-d). And draw its settlement rate curve, as shown in Figure 10 (a ~ d). It can be seen from Fig.10 that the monitoring period of surface subsidence is 9 months, and the subsidence has reached a stable stage. The analysis of Figures 9(c) and 9(d) reveals that the maximum subsidence zone is concentrated near the return airway side of the 3-107 working face, with peak relative subsidence reaching 1,183 mm at monitoring point C31, located approximately 110 meters north of the 3-107 return airway. The surface inclination line demonstrates a southward migration of the maximum subsidence point from the central mining area toward the 3-104 goaf area, with primary subsidence concentration occurring between monitoring points C29 and C35. Relative subsidence decreases progressively toward the southern regions, stabilizing in the central 3-106 mining area and showing minimal change in the southernmost section of the 3-106 mining area. These findings illustrate the complex spatial distribution of surface subsidence, highlighting the influence of adjacent goaf areas and the progressive nature of mining-induced surface deformation.

Analysis of Figures 9(a) and 9(b) reveals distinct subsidence patterns during the monitoring period from October 20, 2023, to July 20, 2024, under the influence of the 3-107 working face mining operations. The maximum relative subsidence of 1,254 mm was recorded at monitoring point A51, located approximately 750 meters east of the cut-eye. The point of maximum subsidence exhibited a progressive eastward migration toward the 2-201 mining goaf area, shifting from its initial position at A43 to its final location at A51 near the 2-201 mining zone. Within the strike monitoring line of the 3-104 mining goaf area, relative subsidence values ranged from 271 to 616 mm (E1-E19), demonstrating that the mining activities of the 3-107 working face significantly influence secondary subsidence phenomena within the large-scale mining goaf area.

In summary, the progressive advancement of the 3-107 working face has induced significant surface subsidence effects across three distinct zones: the immediate vicinity of the 3-107 working face, the 3-104 mining area, and the 3-106 mining area. The inclination monitoring lines reveal that the maximum subsidence is initially concentrated near the return airway side of the 3-107 working face, subsequently migrating from the central region of the 3-107 mining area toward the 3-104 goaf area. Within the 3-106 mining area, relative subsidence demonstrates a gradual stabilization pattern, with minimal changes observed in the central and southern sections. Simultaneously, the strike monitoring lines indicate a progressive eastward migration of the maximum subsidence point toward the 2-201 mining zone. These comprehensive observations demonstrate that the mining activities of the 3-107 working face exert substantial influence on secondary subsidence phenomena within the extensive mining goaf area.

6. CONCLUSIONS

(1) The microseismic monitoring results demonstrate a clear correlation between the advancement of the 3-107 working face and overburden deformation patterns. As the mining distance of the 3-107 working face increases, progressive damage is observed in the overlying strata above adjacent workings, while the rock layers above the 3-106 working face remain relatively unaffected. Furthermore, the analysis reveals a distinct vertical progression of microseismic activity, with events exhibiting an upward migration trend toward higher rock strata as mining operations progress.

(2) The numerical simulation results reveal significant structural changes in response to the continuous advancement of the 3-107 working face. As mining progresses, the overlying strata

above the 3-104 working face experience progressive damage, manifested through three primary indicators: increased roof collapse height, multiplication of interlayer fractures within the large-scale goaf area, and vertical expansion of the fractured zone. These phenomena demonstrate that Continuous Small Pillar Mining induces wave-like propagation of roof movement within the extensive goaf area, significantly influencing the stress distribution and deformation patterns of surrounding rock masses.

(3) The surface subsidence monitoring results demonstrate a progressive expansion of mining-induced impacts corresponding to the advancement of the 3-107 working face. The subsidence effects extend across three primary zones: the immediate vicinity of the 3-107 working face, the 3-104 mining area, and the 3-106 mining area. Analysis of the inclination monitoring lines reveals that the maximum subsidence initially concentrates near the return airway side of the 3-107 working face, subsequently migrating from the central region of the 3-107 mining area toward the 3-104 goaf area. Within the 3-106 mining area, relative subsidence exhibits a gradual stabilization trend. Simultaneously, strike monitoring lines indicate an eastward migration of the maximum subsidence point toward the 2-201 mining zone. These comprehensive observations confirm that the mining activities of the 3-107 working face significantly influence secondary subsidence phenomena within the extensive mining goaf area.

Credit author statement

We declare that we do not have any commercial or associative interest that represents a conflict of interest in connection with the work submitted.

Acknowledgments:

The research described in this paper was financially supported by the Natural Science Foundation of Shanxi Province (No. 202202090301009), which are thankfully acknowledged by the authors.

Declaration of competing interest

The authors declare that they have no known competing financial interests or personal relationships that could have appeared to influence the work reported in this paper.

Data Statement

The data that support the findings of this study are available from [Zhongtian Hechuang Energy Co., Ltd] but restrictions apply to the availability of these data, which were used under license for the current study, and so are not publicly available. Data are however available from the authors upon reasonable request and with permission of [Zhongtian Hechuang Energy Co., Ltd].

Reference:

1. S. Z. Ning, in *2nd International Conference on Energy and Environmental Protection (ICEEP 2013)*. (Guilin, PEOPLES R CHINA, 2013), vol. 734-737, pp. 316-319.
2. L. A. Quan, S. G. Jin, J. X. Zhang, J. Y. Chen, J. J. He, Subsidence Characteristics in North Anhui Coal Mining Areas Using Space-Air-Ground Collaborative Observations. *Sensors* **24**, (2024).
3. P. Strzalkowski, M. Maruszczyk, HARD COAL AS A NECESSARY ENERGY RESOURCE IN POLAND. *Archives of Mining Sciences* **69**, 67-76 (2024).
4. X. P. Diao *et al.*, Combining subsidence theory and slope stability analysis method for building damage assessment in mountainous mining subsidence regions. *Plos One* **14**, (2019).

5. Z. J. Feng, W. B. Guo, F. Y. Xu, D. M. Yang, W. Q. Yang, Control Technology of Surface Movement Scope with Directional Hydraulic Fracturing Technology in Longwall Mining: A Case Study. *Energies* **12**, (2019).
6. S. Y. Ma *et al.*, Surface multi-hazard effect of underground coal mining. *Landslides* **20**, 39-52 (2023).
7. A. A. Malinowska, R. Hejmanowski, THE IMPACT OF DEEP UNDERGROUND COAL MINING ON EARTH FISSURE OCCURRENCE. *Acta Geodynamica Et Geomaterialia* **13**, 321-330 (2016).
8. X. W. Tian, X. Yao, Z. K. Zhou, T. Tao, Surface Multi-Hazard Effects of Underground Coal Mining in Mountainous Regions. *Remote Sensing* **17**, (2025).
9. J. C. Wang *et al.*, A Prediction Method for Surface Subsidence at Deep Mining Areas with Thin Bedrock and Thick Soil Layer Considering Consolidation Behavior. *Natural Resources Research* **33**, 2661-2684 (2024).
10. H. Zhang *et al.*, Overburden breakage and surface damage evolution under high-intensity mining of shallow coal seams: evidence from Shendong mining area. *Scientific Reports* **15**, (2025).
11. Z. L. Mu *et al.*, Study on Surface Damage Induced by High Heavy Layer Movement and Mining-Induced Earthquakes. *Applied Sciences-Basel* **15**, (2025).
12. F. Q. Gao, J. Z. Li, J. F. Lou, S. W. Cao, X. M. Liu, Understanding the evolution of mining-induced fractures using physical and numerical modeling. *Environmental Earth Sciences* **81**, (2022).
13. Q. F. Hu *et al.*, Quantitative and dynamic predictive model for mining-induced movement and deformation of overlying strata. *Engineering Geology* **311**, (2022).
14. K. Tajdus *et al.*, Analysis of Mining-Induced Delayed Surface Subsidence. *Minerals* **11**, (2021).
15. Q. Zhang, J. P. Zou, Y. Y. Jiao, Y. J. Jiang, Q. H. Kou, Mechanism of overburden fracture induced earthquakes in coal seam mining. *Geomechanics and Geophysics for Geo-Energy and Geo-Resources* **10**, (2024).
16. Y. S. Li, C. Zhou, Rockburst Inducement Mechanism and Its Prediction Based on Microseismic Monitoring. *Geofluids* **2021**, (2021).
17. F. Liu, Y. Wang, M. M. Kou, C. H. Liang, Applications of Microseismic Monitoring Technique in Coal Mines: A State-of-the-Art Review. *Applied Sciences-Basel* **14**, (2024).
18. K. K. Wang *et al.*, Study on Deep Mining-Induced Strata Behavior Based on the Evolutional Laws of Multiple Indices from Microseismic Monitoring. *Rock Mechanics and Rock Engineering* **56**, 6481-6501 (2023).
19. Y. Y. Yang, Y. S. Xu, S. L. Shen, Y. Yuan, Z. Y. Yin, Mining-induced geo-hazards with environmental protection measures in Yunnan, China: an overview. *Bulletin of Engineering Geology and the Environment* **74**, 141-150 (2015).
20. K. Zhang, L. Bai, P. F. Wang, Z. Zhu, Field Measurement and Numerical Modelling Study on Mining-Induced Subsidence in a Typical Underground Mining Area of Northwestern China. *Advances in Civil Engineering* **2021**, (2021).
21. T. Y. Tao, J. B. Liu, X. C. Qu, F. Gao, Real-time monitoring rapid ground subsidence using GNSS and Vondrak filter. *Acta Geophysica* **67**, 133-140 (2019).
22. Y. J. Zhang *et al.*, Development Law and Prevention Methods of Mining-induced Ground

Cracks: A Review. *Journal of the Geological Society of India* **101**, 24-41 (2025).